

Article

A left and right truncated Schechter luminosity function for quasars

Lorenzo Zaninetti ¹,¹ Physics Department, via P.Giuria 1,
I-10125 Turin, Italy*Version October 20, 2018 submitted to Galaxies. Typeset by L^AT_EX using class file mdpi.cls*

Abstract: The luminosity function for quasars (QSOs) is usually fitted by a Schechter function. The dependence of the number of quasars on the redshift, both in the low and high luminosity regions, requires the inclusion of a lower and upper boundary in the Schechter function. The normalization of the truncated Schechter function is forced to be the same as that for the Schechter function, and an analytical form for the average value is derived. Three astrophysical applications for QSOs are provided: deduction of the parameters at low redshifts, behavior of the average absolute magnitude at high redshifts, and the location (in redshift) of the photometric maximum as a function of the selected apparent magnitude. The truncated Schechter function with the double power law and an improved Schechter function are compared as luminosity functions for QSOs. The chosen cosmological framework is that of the flat cosmology, for which we provided the luminosity distance, the inverse relation for the luminosity distance, and the distance modulus.

Keywords: Quasars; active or peculiar galaxies, objects, and systems Cosmology

PACS classifications: 98.54.-h 98.80.-k

1. Introduction

The Schechter function was first introduced in order to model the luminosity function (LF) for galaxies, see [1], and later was used to model the LF for quasars (QSOs), see [2,3]. Over the years, other LFs for galaxies have been suggested, such as a two-component Schechter-like LF, see [4], the hybrid Schechter+power-law LF to fit the faint end of the K-band, see [5], and the double Schechter

20 LF, see Blanton *et al.* [6]. In order to improve the flexibility at the bright end, a new parameter η
 21 was introduced in the Schechter LF, see [7]. The above discussion suggests the introduction of finite
 22 boundaries for the Schechter LF rather than the usual zero and infinity. As a practical example the most
 23 luminous QSOs have absolute magnitude $M_{b_j} \approx -28$ or the luminosity is not ∞ and the less luminous
 24 QSOs have absolute magnitude $M_{b_j} \approx -20$ or the luminosity is not zero, see Figure 19 in [8].
 25 A physical source of truncation at the low luminosity boundary (high absolute magnitude) is the fact
 26 that with increasing redshift the less luminous QSOs progressively disappear. In other words the upper
 27 boundary in absolute magnitude for QSOs is function of the redshift.

28 The suggestion to introduce two boundaries in a probability density function (PDF) is not new and, as
 29 an example, [9] considered a doubly-truncated gamma PDF restricted by both a lower (l) and upper (u)
 30 truncation. A way to deduce a new truncated LF for galaxies or QSOs is to start from a truncated PDF
 31 and then to derive the magnitude version. This approach has been used to deduce a left truncated beta
 32 LF, see [10,11], and a truncated gamma LF, see [12].

33 The main difference between LFs for galaxies and for QSOs is that in the first case, we have an LF
 34 for a unit volume of 1 Mpc^3 and in the second case we are speaking of an LF for unit volume but with
 35 a redshift dependence. The dependence on the redshift complicates an analytical approach, because
 36 the number of observed QSOs at low luminosity decreases with the redshift and the highest observed
 37 luminosity increases with the redshift. The first effect is connected with the Malmquist bias, i.e. the
 38 average luminosity increases with the redshift, and the second one can be modeled by an empirical
 39 law. The above redshift dependence in the case of QSOs can be modeled by the double power law LF,
 40 see [13], or by an improved Schechter function, see [14]. The present paper derives, in Section 2, the
 41 luminosity distance and the distance modulus in a flat cosmology. Section 3 derives a truncated version
 42 of the Schechter LF. Section 4 applies the truncated Schechter LF to QSOs, deriving the parameters of
 43 the LF in the range of redshift $[0.3, 0.5]$, modeling the average absolute magnitude as a function of the
 44 redshift, and deriving the photometric maximum for a given apparent magnitude as a function of the
 45 redshift.

46 2. The flat cosmology

The *first* definition of the luminosity distance, d_L , in flat cosmology is

$$d_L(z; c, H_0, \Omega_M) = \frac{c}{H_0} (1+z) \int_{\frac{1}{1+z}}^1 \frac{da}{\sqrt{\Omega_M a + (1 - \Omega_M) a^4}} \quad , \quad (1)$$

where H_0 is the Hubble constant expressed in $\text{km s}^{-1} \text{Mpc}^{-1}$, c is the speed of light expressed in km s^{-1} ,
 z is the redshift, a is the scale-factor, and Ω_M is

$$\Omega_M = \frac{8\pi G \rho_0}{3 H_0^2} \quad , \quad (2)$$

where G is the Newtonian gravitational constant and ρ_0 is the mass density at the present time, see
 eqn (2.1) in [15]. A *second* definition of the luminosity distance is

$$d_L(z; c, H_0, \Omega_M) = \frac{c}{H_0} (1+z) \int_0^z \frac{1}{\sqrt{(1+z)^3 \Omega_M + 1 - \Omega_M}} dz \quad , \quad (3)$$

47 see eqn (2) in [16]. The change of variable $z = -1 + 1/a$ in the second definition allows finding the
 48 first definition. An analytical expression for the integral (1) is here reported as a Taylor series of order 8
 49 when $\Omega_M = 0.3$ and $H_0 = 70 \text{ km s}^{-1} \text{ Mpc}^{-1}$

$$d_L(z) = 4282.74 (1+z)(2.45214 + 0.01506 (1+z)^{-8} - 0.06633 (1+z)^{-7} - 0.01619 (1+z)^{-6} + 0.60913 (1+z)^{-5} - 1.29912 (1+z)^{-4} + 0.406124 (1+z)^{-3} + 2.47428 (1+z)^{-2} - 4.57509 (1+z)^{-1}) \text{ Mpc} \quad (4)$$

50 and the distance modulus as a function of z , $F(z)$,

$$(m - M) = F(z) = 43.15861 + 2.17147 \ln(7.77498 z^2 + 2.45214 z^8 + 15.0420 z^7 + 39.1085 z^6 + 56.4947 z^5 + 49.3673 z^4 + 26.1512 z^3 + 0.99999 z + 1.73 \cdot 10^{-7}) - 15.2003 \ln(1+z) \quad . \quad (5)$$

As a consequence, the absolute magnitude, M , is

$$M = m - F(z) \quad . \quad (6)$$

The angular diameter distance, D_A , after [17], is

$$D_A = \frac{D_L}{(1+z)^2} \quad . \quad (7)$$

We may approximate the luminosity distance as given by eqn (4) by the minimax rational approximation, $d_{L,2,1}$, with the degree of the numerator $p = 2$ and the degree of the denominator $q = 1$:

$$d_{L,2,1}(z) = \frac{4.10871 + 1813.96 z + 2957.04 z^2}{0.44404 + 0.27797 z} \quad (8)$$

51 which allows deriving the inverse formula, the redshift as a function of the luminosity distance:

$$z_{2,1}(d_L) = 0.000047 d_L - 0.306718 + 3.38175 \times 10^{-14} \sqrt{1.9318 \cdot 10^{18} d_L^2 + 1.06093 \times 10^{23} d_L + 8.10464 \times 10^{25}} \quad . \quad (9)$$

Another useful distance is the transverse comoving distance, D_M ,

$$D_M = \frac{D_L}{1+z} \quad , \quad (10)$$

with the connected total comoving volume V_c

$$V_c = \frac{4}{3} \pi D_M^3 \quad , \quad (11)$$

which can be minimax-approximated as

$$V_{c,3,2} = \frac{3.01484 \cdot 10^{10} z^3 + 6.39699 \cdot 10^{10} z^2 - 1.26793 \cdot 10^{10} z + 4.10104 \cdot 10^8}{0.45999 - 0.01011 z + 0.093371 z^2} \text{ Mpc}^3 \quad . \quad (12)$$

52 3. The adopted LFs

This section reviews the Schechter LF, the double power law LF, and the Pei LF for QSOs. The truncated version of the Schechter LF is derived. The merit function χ^2 is computed as

$$\chi^2 = \sum_{j=1}^n \left(\frac{LF_{theo} - LF_{astr}}{\sigma_{LF_{astr}}} \right)^2 , \quad (13)$$

where n is the number of bins for LF of QSOs and the two indices *theo* and *astr* stand for ‘theoretical’ and ‘astronomical’, respectively. The residual sum of squares (RSS) is

$$RSS = \sum_{j=1}^n (y(i)_{theo} - y(i)_{astr})^2 , \quad (14)$$

53 where $y(i)_{theo}$ is the theoretical value and $y(i)_{astr}$ is the astronomical value.

A reduced merit function χ_{red}^2 is evaluated by

$$\chi_{red}^2 = \chi^2 / NF , \quad (15)$$

where $NF = n - k$ is the number of degrees of freedom and k is the number of parameters. The goodness of the fit can be expressed by the probability Q , see equation 15.2.12 in [18], which involves the degrees of freedom and the χ^2 . According to [18], the fit “may be acceptable” if $Q > 0.001$. The Akaike information criterion (AIC), see [19], is defined by

$$AIC = 2k - 2\ln(L) , \quad (16)$$

where L is the likelihood function and k is the number of free parameters in the model. We assume a Gaussian distribution for the errors and the likelihood function can be derived from the χ^2 statistic $L \propto \exp(-\frac{\chi^2}{2})$ where χ^2 has been computed by Equation (13), see [20], [21]. Now the AIC becomes

$$AIC = 2k + \chi^2 . \quad (17)$$

54 3.1. The Schechter LF

Let L be a random variable taking values in the closed interval $[0, \infty]$. The Schechter LF of galaxies, after [1], is

$$\Phi(L; \Phi^*, \alpha, L^*) dL = \left(\frac{\Phi^*}{L^*} \right) \left(\frac{L}{L^*} \right)^\alpha \exp\left(-\frac{L}{L^*}\right) dL , \quad (18)$$

where α sets the slope for low values of L , L^* is the characteristic luminosity, and Φ^* represents the number of galaxies per Mpc^3 . The normalization is

$$\int_0^\infty \Phi(L; \Phi^*, \alpha, L^*) dL = \Phi^* \Gamma(\alpha + 1) , \quad (19)$$

where

$$\Gamma(z) = \int_0^\infty e^{-t} t^{z-1} dt , \quad (20)$$

is the gamma function. The average luminosity, $\langle L \rangle$, is

$$\langle L(\Phi^*, \alpha, L^*) \rangle = L^* \Phi^* \Gamma(\alpha + 2) \quad . \quad (21)$$

An equivalent form in absolute magnitude of the Schechter LF is

$$\Phi(M; \Phi^*, \alpha, M^*) dM = 0.921 \Phi^* 10^{0.4(\alpha+1)(M^*-M)} \exp(-10^{0.4(M^*-M)}) dM, \quad (22)$$

55 where M^* is the characteristic magnitude. The scaling with h is $M^* - 5 \log_{10} h$ and
56 $\Phi^* h^3 [Mpc^{-3}]$.

57 3.2. The truncated Schechter LF

We assume that the luminosity L takes values in the interval $[L_l, L_u]$, where the indices l and u mean ‘lower’ and ‘upper’; the truncated Schechter LF, S_T , is

$$S_T(L; \Psi^*, \alpha, L^*, L_l, L_u) = \frac{-\left(\frac{L}{L^*}\right)^\alpha e^{-\frac{L}{L^*}} \Psi^* \Gamma(\alpha + 1)}{L^* \left(\Gamma\left(\alpha + 1, \frac{L_u}{L^*}\right) - \Gamma\left(\alpha + 1, \frac{L_l}{L^*}\right)\right)}, \quad (23)$$

where $\Gamma(a, z)$ is the incomplete Gamma function defined as

$$\Gamma(a, z) = \int_z^\infty t^{a-1} e^{-t} dt \quad , \quad (24)$$

see [22]. The normalization is the same as for the Schechter LF, see eqn (19),

$$\int_0^\infty S_T(L; \Psi^*, \alpha, L^*, L_l, L_u) dL = \Psi^* \Gamma(\alpha + 1) \quad . \quad (25)$$

The average value is

$$\langle L(\Psi^*, \alpha, L^*, L_l, L_u) \rangle = \frac{N}{L^* \left(\Gamma\left(\alpha + 1, \frac{L_u}{L^*}\right) - \Gamma\left(\alpha + 1, \frac{L_l}{L^*}\right)\right)} \quad (26)$$

58 with

$$N = \Psi^* \left(L^{*2} \Gamma\left(\alpha + 1, \frac{L_u}{L^*}\right) \alpha - L^{*2} \Gamma\left(\alpha + 1, \frac{L_l}{L^*}\right) \alpha + L^{*2} \Gamma\left(\alpha + 1, \frac{L_u}{L^*}\right) - L^{*2} \Gamma\left(\alpha + 1, \frac{L_l}{L^*}\right) - L^{*-\alpha+1} e^{-\frac{L_l}{L^*}} L_l^{\alpha+1} + L^{*-\alpha+1} e^{-\frac{L_u}{L^*}} L_u^{\alpha+1} \right) \Gamma(\alpha + 1) \quad . \quad (27)$$

The four luminosities L, L_l, L^* and L_u are connected with the absolute magnitudes M, M_l, M_u and M^* through the following relationship

$$\frac{L}{L_\odot} = 10^{0.4(M_\odot - M)}, \quad \frac{L_l}{L_\odot} = 10^{0.4(M_\odot - M_u)}, \quad \frac{L^*}{L_\odot} = 10^{0.4(M_\odot - M^*)}, \quad \frac{L_u}{L_\odot} = 10^{0.4(M_\odot - M_l)} \quad (28)$$

59 where the indices u and l are inverted in the transformation from luminosity to absolute magnitude and
60 L_\odot and M_\odot are the luminosity and absolute magnitude of the sun in the considered band. The equivalent
61 form in absolute magnitude of the truncated Schechter LF is therefore

$$\frac{\Psi(M; \Psi^*, \alpha, M^*, M_l, M_u) dM}{\Gamma\left(\alpha + 1, 10^{-0.4M_l + 0.4M^*}\right) - \Gamma\left(\alpha + 1, 10^{0.4M^* - 0.4M_u}\right)} = \frac{-0.4 \left(10^{0.4M^* - 0.4M}\right)^\alpha e^{-10^{0.4M^* - 0.4M}} \Psi^* \Gamma(\alpha + 1) 10^{0.4M^* - 0.4M} (\ln(2) + \ln(5))}{\Gamma\left(\alpha + 1, 10^{-0.4M_l + 0.4M^*}\right) - \Gamma\left(\alpha + 1, 10^{0.4M^* - 0.4M_u}\right)} \quad (29)$$

The averaged absolute magnitude is

$$\langle M(\Psi^*, \alpha, L^*, L_l, L_u) \rangle = \frac{\int_{M_l}^{M_u} M(M; \Psi^*, \alpha, L^*, L_l, L_u) M dM}{\int_{M_l}^{M_u} M(M; \Psi^*, \alpha, L^*, L_l, L_u) dM} . \quad (30)$$

62 3.3. The double power law

The double power law LF for QSOs is

$$\Phi(L; \phi^*, \alpha, \beta, L^*) = \frac{\phi^*}{(L/L^*)^\alpha + (L/L^*)^\beta} , \quad (31)$$

where L^* is the characteristic luminosity, α models the low boundary, and β models the high boundary, see [8,13,23–26]. The magnitude version is

$$\Phi(M; \phi^*, \alpha, \beta, M^*) = \frac{\phi^*}{10^{0.4(\alpha+1)[M-M^*]} + 10^{0.4(\beta+1)[M-M^*]}} , \quad (32)$$

63 where the characteristic absolute magnitude, M^* , and ϕ^* are functions of the redshift.

64 3.4. The Pei function

The exponential $L^{1/4}$ LF, or Pei LF, after [14], is

$$\Phi(L; \phi^*, \beta, L^*) = \frac{\phi^* \left(\frac{L}{L^*}\right)^{-\beta} e^{-\sqrt[4]{\frac{L}{L^*}}}}{L^*} , \quad (33)$$

and the magnitude version is

$$\Phi(M; \phi^*, \beta, M^*) = \frac{0.4 \phi^* \left(\frac{10^{-0.4 M}}{10^{-0.4 M^*}}\right)^{-\beta} e^{-\sqrt[4]{\frac{10^{-0.4 M}}{10^{-0.4 M^*}}}} 10^{-0.4 M} \ln(10)}{10^{-0.4 M^*}} . \quad (34)$$

65 4. The astrophysical applications

66 This section explains the K-correction for QSOs, introduces the sample of QSOs on which the various
67 tests are performed, finds the parameters of the new LF in the range of redshift [0.3, 0.5], and finds the
68 number of QSOs as a function of the redshift.

69 4.1. K-correction

The K-correction for QSOs as a function of the redshift can be parametrized as

$$K(z) = -2.5(1 + \alpha_\nu) \log(1 + z) , \quad (35)$$

with $-0.7 < \alpha_\nu < -0.3$, see [27]. Following [28], we have adopted $\alpha_\nu = -0.3$. The corrected absolute magnitude, M_K , is

$$M_K = M + K(z) . \quad (36)$$

70 In the following, both the observed and the theoretical absolute magnitude will always be K-corrected.

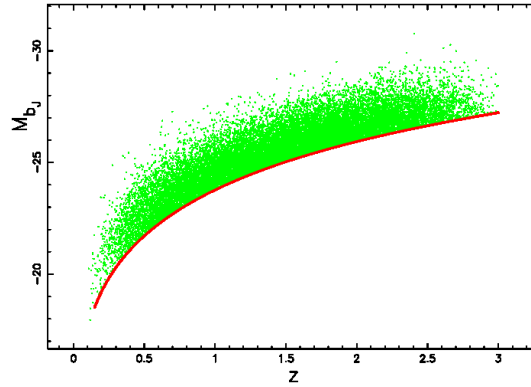


Figure 1. The absolute magnitude $M_{B_{b_j}}$ computed with the nonlinear Eq. (36) for 22413 QSOs versus the redshift, (green points). The lower theoretical curve (upper absolute magnitude) as represented by the nonlinear Eq. (37) is the red thick line. The redshifts cover the range $[0, 3]$

71 4.2. The sample of QSO

We selected the catalog of the 2dF QSO Redshift Survey (2QZ), which contains 22431 redshifts of QSOs with $18.25 < b_J < 20.85$, a total survey area of 721.6 deg^2 , and an effective area of 673.4 deg^2 , see [8]¹. Section 3 in [8] discusses four separate types of completeness which characterize the 2QZ and 6QZ surveys: (i) morphological completeness, $f_m(b_J, z)$, (ii) photometric completeness, $f_p(b_J, z)$, (iii) coverage completeness $f_c(\theta)$ and (iv) spectroscopic completeness, $f_s(b_J, z, \theta)$. The first test can be done on the upper limit of the maximum absolute magnitude, $M_u(z)$, which can be observed in a catalog of QSOs characterized by a given limiting magnitude, in our case $b_j = 20.85$, where $F(z)$ has been defined by eqn (5):

$$M_u(z) = 20.85 - F(z) \quad , \quad (37)$$

72 see Figure 1.

73 A careful examination of Figure 1 allows concluding that all the QSOs are in the region over the border
74 line, the number of observed QSOs decreases with increasing z , and the average absolute magnitude
75 decreases with increasing z . The previous comments can be connected with the Malmquist bias, see
76 [29,30], which was originally applied to the stars and later on to the galaxies by [31].

77 4.3. The luminosity function for QSOs

78 A binned luminosity function for quasars can be built in one of the two methods suggested by [32]:
79 the $\frac{1}{V_a}$ method, see [33–35], and a binned approximation. Notably, [36], argued that both the $\frac{1}{V_a}$ and
80 the binned approximation can produce bias at the faint end of the LF due to the arbitrary choosing of
81 redshift and luminosity intervals.

¹ Data at <http://vizier.u-strasbg.fr/viz-bin/VizieR?-source=VII/241>.

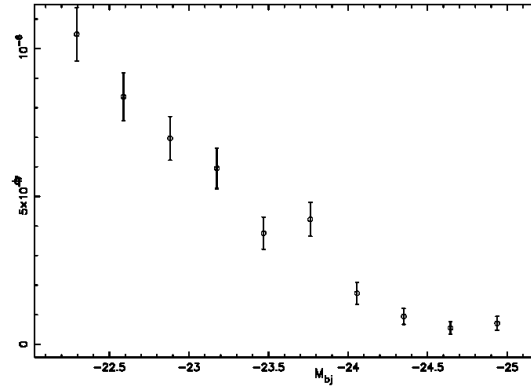


Figure 2. The observed LF for QSOs is reported with the error bar evaluated as the square root of the LF (Poissonian distribution) when $z \in [0.3, 0.5]$.

We implemented the binned approximation of [32], ϕ_{est} , as

$$\phi \approx \phi_{est} = \frac{N_q}{\int_{M_{min}}^{M_{max}} \int_{z_{min}}^{z_{max}(M)} \frac{dV}{dz} dz dM} \quad , \quad (38)$$

where N_q is the number of quasars observed in the $M_i - z$ bin. The error is evaluated as

$$\delta\phi_{est} = \frac{\sqrt{N_q}}{\int_{M_{min}}^{M_{max}} \int_{z_{min}}^{z_{max}(M)} \frac{dV}{dz} dz dM} \quad . \quad (39)$$

The comoving volume in the flat cosmology is evaluated according to equation (11),

$$V = \frac{4}{3}\pi(D_{M,upp}^3 - D_{M,low}^3) \quad , \quad (40)$$

where $D_{M,upp}$ and $D_{M,low}$ are, respectively, the upper and lower comoving distance. A correction for the effective volume of the catalog, V_q , gives

$$V_q = V \frac{A_e \text{ deg}^2}{41252.9 \text{ deg}^2} \quad , \quad (41)$$

82 where A_e is the effective area of the catalog in deg^2 .

83 A typical example of the observed LF for QSOs when $0.3 < z < 0.5$ is reported in Figure 2 and
84 Figure 3 reports the LF for QSOs in four ranges of redshift.

85 The variable lower bound in absolute magnitude, M_l can be connected with evolutionary effects, and
86 the upper bound, M_u , is fixed by the physics, see the nonlinear Eq. (37), see Section 4.4.

87 The five parameters of the the best fit to the observed LF by the truncated Schechter LF can be found
88 with the Levenberg–Marquardt method and are reported in Table 1. The resulting fitted curve is displayed
89 in Figure 4.

90 For the sake of comparison, Table 2 reports the three parameters of the Schechter LF.

91 As a *first* reference the fit with the double power LF, see equation (32), is displayed in Figure 5 with
92 parameters as in Table 3.

93 As a *second* reference the fit with the Pei LF, see equation (34), is displayed in Figure 6 with
94 parameters as in Table 3.

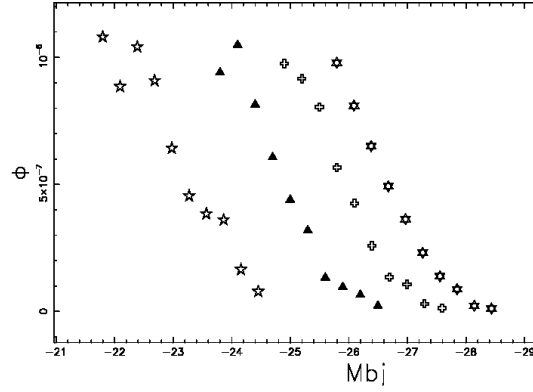


Figure 3. The observed LF for QSOs when z [0.3, 0.5] and M [-24.45, -21.50] (empty stars), [0.7, 0.9] and M [-26.49, -23.50] (full triangles), [1.1, 1.3] and M [-27.59, -24.60] (empty crosses) and [1.5, 1.7] and M [-28.43, -25.50] (stars of David).

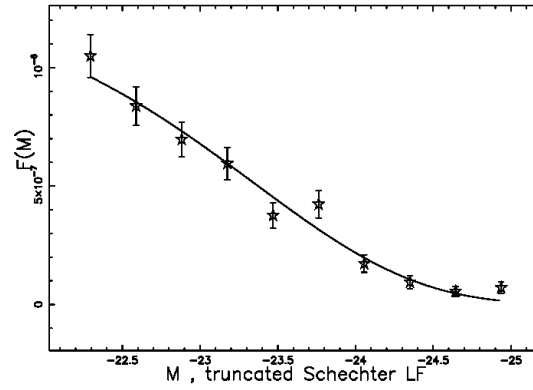


Figure 4. The observed LF for QSOs, empty stars with error bar, and the fit by the truncated Schechter LF when z [0.3, 0.5] and M [-24.93, -22].

Table 1. Parameters of the truncated Schechter LF in the range of redshifts [0.3, 0.5] when $n=10$ and $k=5$.

| M_l | M^* | M_u , | Ψ^* | α | χ^2 | χ_{red}^2 | Q | AIC |
|--------|--------|---------|----------------------|----------|----------|----------------|-------|-------|
| -24.93 | -23.28 | -22.29 | $3.38 \cdot 10^{-8}$ | -0.97 | 12.89 | 2.57 | 0.024 | 22.89 |

Table 2. Parameters of the Schechter LF in the range [0.3, 0.5] when $k=3$ and $n=10$.

| M^* | Ψ^* | α | χ^2 | χ_{red}^2 | Q | AIC |
|--------|----------------------|----------|----------|----------------|-------|-------|
| -23.75 | $8.85 \cdot 10^{-7}$ | -1.37 | 10.49 | 1.49 | 0.162 | 16.49 |

Table 3. Parameters of the double power LF in the range of redshifts [0.3, 0.5] when $n=10$ and $k=4$.

| M^* | ϕ^* | α | β | χ^2 | χ_{red}^2 | Q | AIC |
|--------|----------------------|----------|---------|----------|----------------|------|-------|
| -23.82 | $5.44 \cdot 10^{-7}$ | -3.57 | -1.48 | 9.44 | 1.57 | 0.15 | 17.44 |

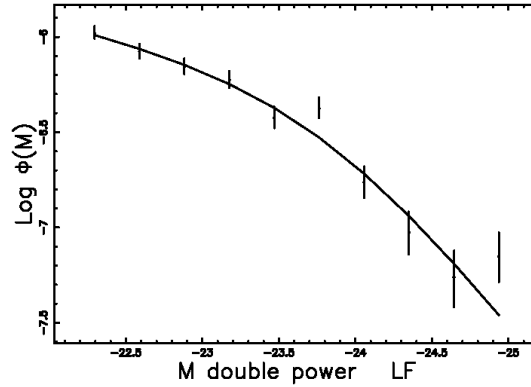


Figure 5. The observed LF for QSOs, empty stars with error bar, and the fit by the double power LF when the redshifts cover the range $[0.3, 0.5]$

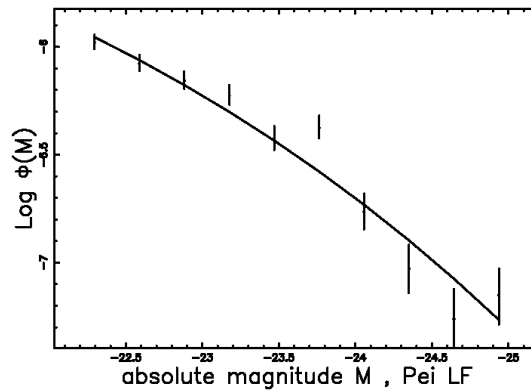


Figure 6. The observed LF for QSOs, empty stars with error bar, and the fit by the Pei LF when the redshifts cover the range $[0.3, 0.5]$

Table 4. Parameters of the Pei LF in the range of redshifts $[0.3, 0.5]$ with $k=3$ and $n=10$.

| M^* | ϕ^* | β | χ^2 | χ^2_{red} | Q | AIC |
|--------|----------------------|---------|----------|----------------|-------|-------|
| -16.47 | $3.68 \cdot 10^{-5}$ | 0.924 | 14.4 | 2.05 | 0.044 | 20.40 |

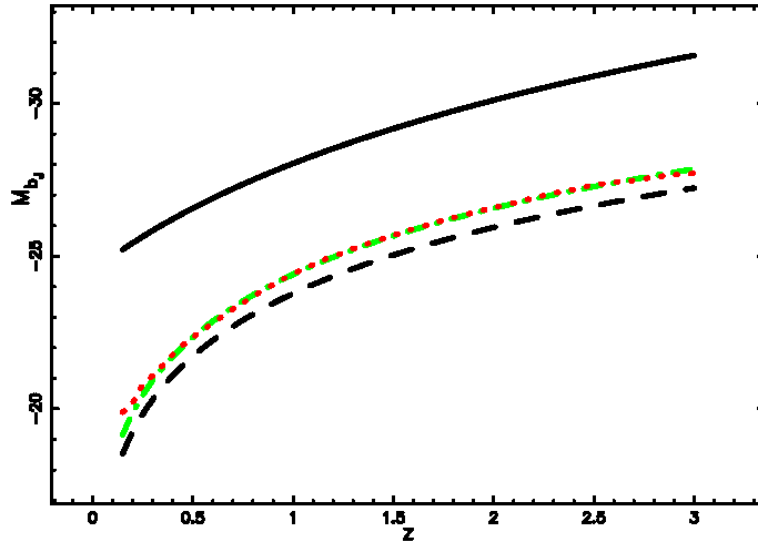


Figure 7. Average observed absolute magnitude versus redshift for QSOs (red points), average theoretical absolute magnitude for truncated Schechter LF as given by eqn (30) (dot-dash-dot green line), theoretical curve for the empirical lowest absolute magnitude at a given redshift, see eqn (42) (full black line) and the theoretical curve for the highest absolute magnitude at a given redshift (dashed black line), see eqn (37), RSS=1.212.

95 4.4. Evolutionary effects

In order to model the evolutionary effects, an empirical variable lower bound in absolute magnitude, M_l , has been introduced,

$$M_l(z) = -24.5 - 10 \times \log_{10}(1 + z) + K(z) \quad . \quad (42)$$

The above empirical formula is classified as top line in Figure 5 of [28] and connected with the limits in magnitude. Conversely the upper bound, M_u was already fixed by the nonlinear Eq. (37). A second evolutionary correction is

$$M^* = M_u(z) - 0.5 \quad , \quad (43)$$

96 where $M_u(z)$ has been defined in eqn (37). Figure 7 reports a comparison between the theoretical and the
 97 observed average absolute magnitudes; the value of M^* reported in eqn (43) minimizes the difference
 98 between the two curves.

As a *first* reference Figure 8 reports a comparison between the theoretical and the observed average absolute magnitudes in the case of the double power LF; the value of M^* which minimizes the difference between the two curves

$$M^* = M_u(z) - 0.4 \quad , \quad (44)$$

99 and other parameters as in Table 3.

100 As a *second* reference Figure 9 reports a comparison between the theoretical and the observed average
 101 absolute magnitude in the case of the Pei LF with parameters as in Table 4.

102 In the above fit, the evolutionary correction for M^* is absent.

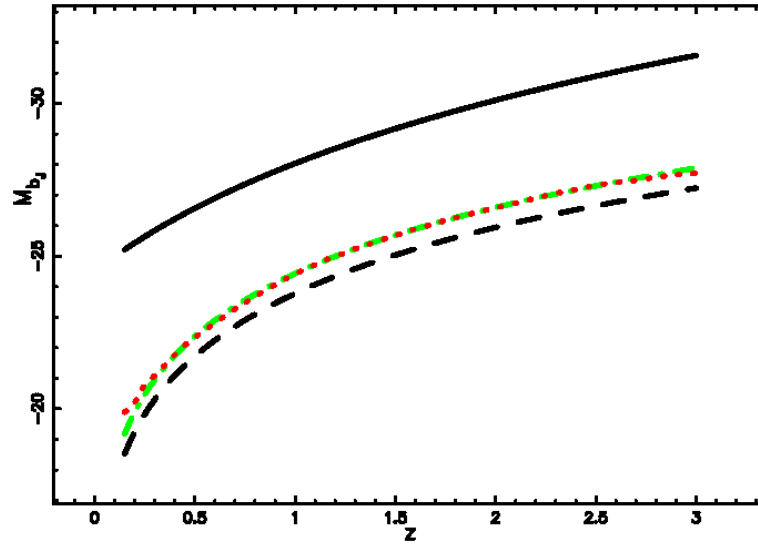


Figure 8. Average observed absolute magnitude versus redshift for QSOs (red points), average theoretical absolute magnitude for the double power LF as evaluated numerically (dot-dash-dot green line), theoretical curve for the empirical lowest absolute magnitude at a given redshift, see eqn (42) (full black line) and the theoretical curve for the highest absolute magnitude at a given redshift (dashed black line), see eqn (37), RSS= 1.138.

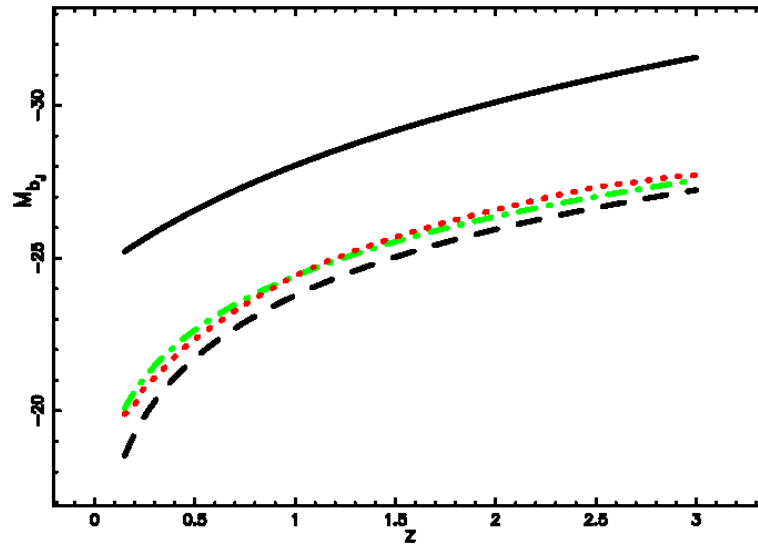


Figure 9. Average observed absolute magnitude versus redshift for QSOs (red points), average theoretical absolute magnitude for the Pei LF as evaluated numerically (dot-dash-dot green line), theoretical curve for the empirical lowest absolute magnitude at a given redshift, see eqn (42) (full black line) and the theoretical curve for the highest absolute magnitude at a given redshift (dashed black line), see eqn (37), RSS= 5.41.

103 4.5. The photometric maximum

The definition of the flux, f , is

$$f = \frac{L}{4\pi r^2} \quad , \quad (45)$$

where r is the luminosity distance. The redshift is approximated as

$$z = z_{2,1} \quad , \quad (46)$$

where $z_{2,1}$ has been introduced into eqn (9). The relation between dr and dz is

$$dr = \frac{(2626.1 z + 821.99 z^2 + 804.33)}{(0.44404 + 0.27797 z)^2} dz \quad , \quad (47)$$

where r has been defined as $d_{L,2,1}$ by the minimax rational approximation, see eqn (8). The joint distribution in z and f for the number of galaxies is

$$\frac{dN}{d\Omega dz df} = \frac{1}{4\pi} \int_0^\infty 4\pi r^2 dr S_T(L; \Psi^*, \alpha, L^*, L_l, L_u) \delta(z - (z_{2,1})) \delta\left(f - \frac{L}{4\pi r^2}\right) \quad , \quad (48)$$

where δ is the Dirac delta function and $S_T(L; \Psi^*, \alpha, L^*, L_l, L_u)$ has been defined in eqn (23). The above formula has the following explicit version

$$\frac{dN}{d\Omega dz df} = \frac{NL}{DL} \quad , \quad (49)$$

104 where

$$NL = -1.71174 \times 10^{21} (z + 0.61116)^4 (z + 0.00227)^4 \times \left(1.422 \cdot 10^9 \frac{f (z + 0.61116)^2 (z + 0.00227)^2}{(z + 1.59739)^2 L^*} \right)^\alpha e^{-1.422 \cdot 10^9 \frac{f (z + 0.61116)^2 (z + 0.00227)^2}{(z + 1.59739)^2 L^*}} \times \Psi^* \Gamma(\alpha + 1) (z + 2.85165) (z + 0.343138) \quad (50)$$

105 where

$$DL = (z + 1.59739)^6 L^* \left(\Gamma\left(\alpha + 1, \frac{L_u}{L^*}\right) - \Gamma\left(\alpha + 1, \frac{L_l}{L^*}\right) \right) \quad . \quad (51)$$

106 The magnitude version is

$$\frac{dN}{d\Omega dz dm} = \frac{NM}{DM} \quad , \quad (52)$$

107 with

$$NM = -1.25459 \times 10^{30} (z + 0.61116)^4 (z + 0.00227)^4 \times \left(1.13159 \times 10^{18} \frac{e^{0.92103 M_\odot - 0.92103 m} (z + 0.61116)^2 (z + 0.00227)^2}{(z + 1.59739)^2 10^{0.4 M_\odot - 0.4 M^*}} \right)^\alpha \times e^{-1.13159 \times 10^{18} \frac{e^{0.92103 M_\odot - 0.92103 m} (z + 0.61116)^2 (z + 0.00227)^2}{(z + 1.59739)^2 10^{0.4 M_\odot - 0.4 M^*}}} \times \Psi^* \Gamma(\alpha + 1.0) (z + 2.85165) (z + 0.34313) e^{0.92103 M_\odot - 0.92103 m} \quad (53)$$

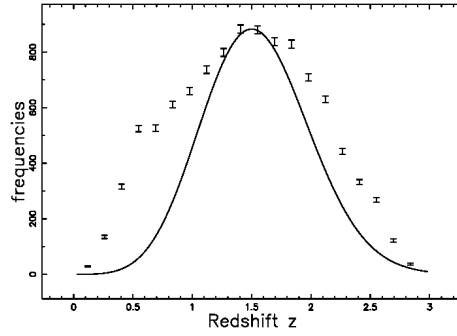


Figure 10. The QSOs with $20.16 \leq m \leq 20.85$ are organized in frequencies versus spectroscopic redshift, points with error bar. The redshifts cover the range $[0, 3]$ and the histogram's interval is 0.14. The maximum frequency of observed QSOs is at $z = 1.478$ and the number of bins is 20. The full line is the theoretical curve generated by $\frac{dN}{d\Omega dz dm}(z)$ as given by the application of the truncated Schechter LF which is Eq. (52) with parameters as in Table 1 but $M^* = -22.5$. The theoretical maximum is at $z = 1.491$.

108 and

$$DM = (z + 1.59739)^6 10^{0.4 M_\odot - 0.4 M^*} \times \left(\Gamma \left(\alpha + 1, \frac{10^{0.4 M_\odot - 0.4 M_l}}{10^{0.4 M_\odot - 0.4 M^*}} \right) - \Gamma \left(\alpha + 1, \frac{10^{0.4 M_\odot - 0.4 M_u}}{10^{0.4 M_\odot - 0.4 M^*}} \right) \right), \quad (54)$$

where m is the apparent magnitude of the catalog, the absolute magnitudes M_l , M_u , M^* and M_\odot have been defined in Section 3.2. The conversion from flux, f , to apparent magnitude, m , in the above formula is obtained from the usual formula

$$f = 7.95774 \times 10^8 e^{0.92103 M_\odot - 0.92103 m}, \quad (55)$$

and

$$df = -7.32935 \times 10^8 e^{0.92103 M_\odot - 0.92103 m} dm. \quad (56)$$

109 The number of galaxies in z and m as given by formula (52) has a maximum at $z = z_{pos-max}$ but there
 110 is no analytical solution for such a position and a numerical analysis should be performed. Figure 10
 111 reports the observed and the theoretical number of QSOs as functions of the redshift at a given apparent
 112 magnitude when $M_l(z)$ is given by eqn (42) and $M_u(z)$ is given by eqn (37). Here we adopted the law
 113 of rare events, i.e. the Poisson distribution, in which the variance is equal to the mean, i.e. the error bar
 114 is given by the square root of the frequency.

115 In the above fit the observed position of the maximum, $z = 1.478$, and the theoretical prediction,
 116 $z = 1.491$, have approximately the same value. In the two regions surrounding the maximum, the degree
 117 of prediction is not as accurate, due to the fact that the three absolute magnitudes M_l , M_u and M^* are
 118 functions of z .

119 5. Conclusions

120 Absolute Magnitude

121 The evaluation of the absolute magnitude of a QSO is connected with the distance modulus, which,
 122 in the case of the flat cosmology, ($\Omega_M = 0.3$, $H_0 = 70 \text{ km s}^{-1} \text{ Mpc}^{-1}$) is reported in eqn (5) as a Taylor
 123 series of order 8 with range in z , $[0 - 4]$. As an application of the above series, we derived an inverse
 124 formula for the redshift as a function of the luminosity distance and an approximate formula for the total
 125 comoving volume.

126 **Truncated Schechter LF**

127 The Schechter LF is characterized by three parameters: Φ^* , α and M^* . The truncated Schechter LF
 128 is characterized by five parameters: Ψ^* , α , M^* , M_l and M_u . The reference LF for QSOs, the double
 129 power law LF, is characterized by four parameters: ϕ^* , α , β and M^* . An application of the above LFs in
 130 the range of z $[0.3, 0.5]$ gives the following reduced chi-square $\chi_{red}^2 = 2.57$ for the truncated Schechter
 131 LF, $\chi_{red}^2 = 1.49$ for the Schechter LF, $\chi_{red}^2 = 1.57$ for the double power LF, and $\chi_{red}^2 = 2.05$ for the Pei
 132 LF. The other statistical such as the AIC are reported in Tables 1, 2, 3, and 4. We can therefore speak
 133 of minimum differences between the four LFs here analyzed in the nearby universe defined by redshifts
 134 $[0.3, 0.5]$.

135 **Evolutionary effects**

136 The evolution of the LF for QSOs as a function of the redshift is here modeled by an upper and lower
 137 truncated Schechter function. This choice allows modeling the lower bound in luminosity (the higher
 138 bound in absolute magnitude) according to the evolution of the absolute magnitude, see Eq. (37). The
 139 evaluation of the upper bound in luminosity (the lower bound in absolute magnitude) is empirical and
 140 is reported in eqn (42). A variable value of M^* with z in the case of the truncated Schechter LF, see
 141 eqn (43), allows matching the evolution of the observed average value of absolute magnitude with the
 142 theoretical average value of absolute magnitude, see Figure 7. A comparison is done with the theoretical
 143 average value in absolute magnitude for the case of a double power law and the Pei function, see Figures
 144 8 and 9.

145 **Maximum in magnitude**

146 The joint distribution in redshift and energy flux density is here modeled in the case of a flat universe,
 147 see formula 48. The position in redshift of the maximum in the number of galaxies for a given flux or
 148 apparent magnitude does not have an analytical expression and is therefore found numerically, see Figure
 149 10. A comparison can be done with the number of galaxies as a function of the redshift in $[0 - 0.3]$ for
 150 the 2dF Galaxy Redshift Survey in the South and North galactic poles, see Figure 6 in [37] where the
 151 theoretical model is obtained by the generation of random catalogs.

152 **References**

- 153 1. Schechter, P. An analytic expression for the luminosity function for galaxies. *ApJ* **1976**,
 154 *203*, 297–306.
- 155 2. Warren, S.J.; Hewett, P.C.; Osmer, P.S. A wide-field multicolor survey for high-redshift quasars,
 156 Z greater than or equal to 2.2. 3: The luminosity function. *ApJ* **1994**, *421*, 412–433.
- 157 3. Goldschmidt, P.; Miller, L. The UVX quasar optical luminosity function and its evolution.
 158 *MNRAS* **1998**, *293*, 107, [[astro-ph/9709019](#)].
- 159 4. Driver, S.P.; Phillipps, S. Is the Luminosity Distribution of Field Galaxies Really Flat? *ApJ*
 160 **1996**, *469*, 529–534.

- 161 5. Bell, E.F.; McIntosh, D.H.; Katz, N.; Weinberg, M.D. The Optical and Near-Infrared Properties
162 of Galaxies. I. Luminosity and Stellar Mass Functions. *ApJS* **2003**, *149*, 289–312,
163 [[astro-ph/0302543](#)].
- 164 6. Blanton, M.R.; Lupton, R.H.; Schlegel, D.J.; Strauss, M.A.; Brinkmann, J.; Fukugita, M.;
165 Loveday, J. The Properties and Luminosity Function of Extremely Low Luminosity Galaxies.
166 *ApJ* **2005**, *631*, 208–230.
- 167 7. Alcaniz, J.S.; Lima, J.A.S. Galaxy Luminosity Function: A New Analytic Expression. *Brazilian*
168 *Journal of Physics* **2004**, *34*, 455–458.
- 169 8. Croom, S.M.; Smith, R.J.; Boyle, B.J.; Shanks, T.; Miller, L.; Outram, P.J.; Loring, N.S. The
170 2dF QSO Redshift Survey - XII. The spectroscopic catalogue and luminosity function. *MNRAS*
171 **2004**, *349*, 1397–1418, [[astro-ph/0403040](#)].
- 172 9. Coffey, C.S.; Muller, K.E. Properties of doubly-truncated gamma variables. *Communications in*
173 *Statistics - Theory and Methods* **2000**, *29*, 851–857.
- 174 10. Zaninetti, L. The Luminosity Function of Galaxies as Modeled by a Left Truncated Beta
175 Distribution. *International Journal of Astronomy and Astrophysics* **2014**, *4*, 145–154,
176 [[arXiv:astro-ph.CO/1403.2558](#)].
- 177 11. Zaninetti, L. On the Number of Galaxies at High Redshift. *Galaxies* **2015**, *3*, 129–155.
- 178 12. Zaninetti, L. Pade Approximant and Minimax Rational Approximation in Standard Cosmology.
179 *Galaxies* **2016**, *4*, 4–24.
- 180 13. Boyle, B.J.; Shanks, T.; Peterson, B.A. The evolution of optically selected QSOs. II. *MNRAS*
181 **1988**, *235*, 935–948.
- 182 14. Pei, Y.C. The luminosity function of quasars. *ApJ* **1995**, *438*, 623–631.
- 183 15. Adachi, M.; Kasai, M. An Analytical Approximation of the Luminosity Distance in
184 Flat Cosmologies with a Cosmological Constant. *Progress of Theoretical Physics* **2012**,
185 *127*, 145–152.
- 186 16. Mészáros, A.; Řípa, J. A curious relation between the flat cosmological model and the elliptic
187 integral of the first kind. *A&A* **2013**, *556*, A13.
- 188 17. Etherington, I.M.H. On the Definition of Distance in General Relativity. *Philosophical Magazine*
189 **1933**, *15*.
- 190 18. Press, W.H.; Teukolsky, S.A.; Vetterling, W.T.; Flannery, B.P. *Numerical Recipes in FORTRAN.*
191 *The Art of Scientific Computing*; Cambridge University Press: Cambridge, UK, 1992.
- 192 19. Akaike, H. A new look at the statistical model identification. *IEEE Transactions on Automatic*
193 *Control* **1974**, *19*, 716–723.
- 194 20. Liddle, A.R. How many cosmological parameters? *MNRAS* **2004**, *351*, L49–L53.
- 195 21. Godlowski, W.; Szydowski, M. Constraints on Dark Energy Models from Supernovae.
196 1604-2004: Supernovae as Cosmological Lighthouses; Turatto, M.; Benetti, S.; Zampieri, L.;
197 Shea, W., Eds., 2005, Vol. 342, *Astronomical Society of the Pacific Conference Series*, pp.
198 508–516.
- 199 22. Olver, F.W.J.e.; Lozier, D.W.e.; Boisvert, R.F.e.; Clark, C.W.e. *NIST handbook of mathematical*
200 *functions.*; Cambridge University Press. : Cambridge, 2010.

- 201 23. Boyle, B.J.; Shanks, T.; Croom, S.M.; Smith, R.J.; Miller, L.; Loaring, N.; Heymans, C. The
202 2dF QSO Redshift Survey - I. The optical luminosity function of quasi-stellar objects. *MNRAS*
203 **2000**, *317*, 1014–1022, [[astro-ph/0005368](#)].
- 204 24. Richards, G.T.; Strauss, M.A.; Fan, X.; Hall, P.B.; Jester, S.; Schneider, D.P.; Vanden Berk, D.E.;
205 Stoughton, C.; Anderson, S.F.; Brunner, R.J.; Gray, J.; Gunn, J.E.; Ivezić, Ž.; Kirkland, M.K.;
206 Knapp, G.R.; Loveday, J.; Meiksin, A.; Pope, A.; Szalay, A.S.; Thakar, A.R.; Yanny, B.; York,
207 D.G.; Barentine, J.C.; Brewington, H.J.; Brinkmann, J.; Fukugita, M.; Harvanek, M.; Kent, S.M.;
208 Kleinman, S.J.; Krzesiński, J.; Long, D.C.; Lupton, R.H.; Nash, T.; Neilsen, Jr., E.H.; Nitta, A.;
209 Schlegel, D.J.; Snedden, S.A. The Sloan Digital Sky Survey Quasar Survey: Quasar Luminosity
210 Function from Data Release 3. *AJ* **2006**, *131*, 2766–2787, [[astro-ph/0601434](#)].
- 211 25. Ross, N.P.; McGreer, I.D.; White, M.; Richards, G.T.; Myers, A.D.; Palanque-Delabrouille, N.;
212 Strauss, M.A.; Anderson, S.F.; Shen, Y.; Brandt, W.N.; Yèche, C.; Swanson, M.E.C.; Aubourg,
213 É.; Bailey, S.; Bizyaev, D.; Bovy, J.; Brewington, H.; Brinkmann, J.; DeGraf, C.; Di Matteo, T.;
214 Ebelke, G.; Fan, X.; Ge, J.; Malanushenko, E.; Malanushenko, V.; Mandelbaum, R.; Maraston,
215 C.; Muna, D.; Oravetz, D.; Pan, K.; Pâris, I.; Petitjean, P.; Schawinski, K.; Schlegel, D.J.;
216 Schneider, D.P.; Silverman, J.D.; Simmons, A.; Snedden, S.; Streblyanska, A.; Suzuki, N.;
217 Weinberg, D.H.; York, D. The SDSS-III Baryon Oscillation Spectroscopic Survey: The Quasar
218 Luminosity Function from Data Release Nine. *ApJ* **2013**, *773*, 14, [[1210.6389](#)].
- 219 26. Singh, S.A. Optical Luminosity Function of Quasi Stellar Objects. *American Journal of*
220 *Astronomy and Astrophysics* **2016**, *4*, 78.
- 221 27. Wisotzki, L. Quasar spectra and the K correction. *A&A* **2000**, *353*, 861–866.
- 222 28. Croom, S.M.; Richards, G.T.; Shanks, T.; Boyle, B.J.; Strauss, M.A.; Myers, A.D.; Nichol,
223 R.C.; Pimblet, K.A.; Ross, N.P.; Schneider, D.P.; Sharp, R.G.; Wake, D.A. The 2dF-SDSS
224 LRG and QSO survey: the QSO luminosity function at z between 0.4 and 2.6. *MNRAS* **2009**,
225 *399*, 1755–1772, [[0907.2727](#)].
- 226 29. Malmquist, K. A study of the stars of spectral type A. *Lund Medd. Ser. II* **1920**, *22*, 1–10.
- 227 30. Malmquist, K. On some relations in stellar statistics. *Lund Medd. Ser. I* **1922**, *100*, 1–10.
- 228 31. Behr, A. Zur Entfernungsskala der extragalaktischen Nebel. *Astronomische Nachrichten* **1951**,
229 *279*, 97–107.
- 230 32. Page, M.J.; Carrera, F.J. An improved method of constructing binned luminosity functions.
231 *MNRAS* **2000**, *311*, 433–440, [[astro-ph/9909434](#)].
- 232 33. Avni, Y.; Bahcall, J.N. On the simultaneous analysis of several complete samples - The V/V_{\max}
233 and V_e/V_a variables, with applications to quasars. *ApJ* **1980**, *235*, 694–716.
- 234 34. Eales, S. Direct construction of the galaxy luminosity function as a function of redshift. *ApJ*
235 **1993**, *404*, 51–62.
- 236 35. Ellis, R.S.; Colless, M.; Broadhurst, T.; Heyl, J.; Glazebrook, K. Autofib Redshift Survey - I.
237 Evolution of the galaxy luminosity function. *MNRAS* **1996**, *280*, 235–251, [[astro-ph/9512057](#)].
- 238 36. Yuan, Z.; Wang, J. A graphical analysis of the systematic error of classical binned methods
239 in constructing luminosity functions. *Astrophysics and Space Science* **2013**, *345*, 305–313,
240 [[arXiv:astro-ph.IM/1302.5887](#)].

241 37. Cole, S.; Percival, W.J.; Peacock, J.A.; Norberg, P.; Baugh, C.M.; Frenk, C.S.; Baldry, I.;
242 Bland-Hawthorn, J.; Bridges, T.; Cannon, R.; Colless, M.; Collins, C.; Couch, W.; Cross, N.J.G.;
243 Dalton, G.; Eke, V.R.; De Propris, R.; Driver, S.P.; Efstathiou, G.; Ellis, R.S.; Glazebrook,
244 K.; Jackson, C.; Jenkins, A.; Lahav, O.; Lewis, I.; Lumsden, S.; Maddox, S.; Madgwick, D.;
245 Peterson, B.A.; Sutherland, W.; Taylor, K. The 2dF Galaxy Redshift Survey: power-spectrum
246 analysis of the final data set and cosmological implications. *MNRAS* **2005**, *362*, 505–534,
247 [\[astro-ph/0501174\]](https://arxiv.org/abs/astro-ph/0501174).

248 © October 20, 2018 by the author; submitted to *Galaxies* for possible open access
249 publication under the terms and conditions of the Creative Commons Attribution license
250 <http://creativecommons.org/licenses/by/4.0/>.